JACS
JOURNAL OF THE AMERICAN CHEMICAL SOCIETY
Article
pubs.acs.org/JACS

A Mechanistic Study of Halogen Addition and Photoelimination from π-Conjugated Tellurophenes

Elisa I. Carrera,[†] Anabel E. Lanterna,[‡] Alan J. Lough,[†] Juan C. Scaiano,*[,‡] and Dwight S. Seferos*[,†]

[†]Department of Chemistry, University of Toronto, 80 St. George Street, Toronto, Ontario M5S 3H6, Canada

[‡]Department of Chemistry and Centre for Catalysis Research and Innovation, University of Ottawa, 10 Marie Curie, Ottawa, Ontario K1N 6N5, Canada

Supporting Information

ABSTRACT: The ability to drive reactivity using visible light is of importance for many disciplines of chemistry and has significant implications for sustainable chemistry. Identifying photochemically active compounds and understanding photochemical mechanisms is important for the development of useful materials for synthesis and catalysis. Here we report a series of photoactive diphenyltellurophene compounds bearing electron-withdrawing and electron-donating substituents synthesized by alkyne coupling/ring closing or palladium-catalyzed ipso-arylation chemistry. The redox chemistry of these compounds was studied with respect to oxidative addition and photoelimination of bromine, which is of importance for energy storage reactions involving X_2. The oxidative addition reaction mechanism was studied using density functional theory, the results of which support a three-step mechanism involving the formation of an initial η^1 association complex, a monobrominated intermediate, and finally the dibrominated product. All of the tellurophene derivatives undergo photoreduction using 430, 447, or 617 nm light depending on the absorption properties of the compound. Compounds bearing electron-withdrawing substituents have the highest photochemical quantum efficiencies in the presence of an alkene trap, with efficiencies of up to 42.4% for a pentafluorophenyl-functionalized tellurophene. The photoelimination reaction was studied in detail through bromine trapping experiments and laser flash photolysis, and a mechanism is proposed. The photoreaction, which occurs by release of bromine radicals, is competitive with intersystem crossing to the triplet state of the brominated species, as evidenced by the formation of singlet oxygen. These findings should be useful for the design of new photochemically active compounds supported by main-group elements.

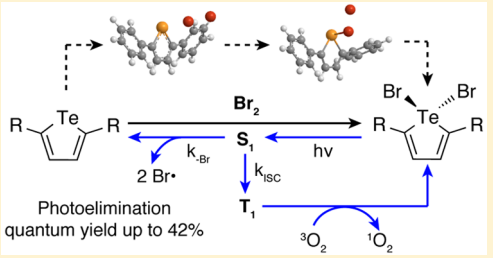

1. INTRODUCTION

Light-driven chemical reactions are important for many disciplines of chemistry, including synthesis and catalysis, because of the relatively low energy input (especially when visible light is used) and the ability to access reaction pathways that are not accessible by thermal activation.[1] Photochemistry has significant implications for sustainable chemistry and renewable energy. The use of light to drive fuel production reactions such as H_2O and HX splitting is becoming increasingly important.[2−6] Several dinuclear late transition metal complexes efficiently photoeliminate halogens, which is the turnover-limiting step in the HX-splitting catalytic cycle. Some of these include Pt−Au,[7] Ir−Au,[8] Au−Au,[9] Pt−Rh,[10] Rh−Rh,[11] and Pt−Pt complexes (Chart 1).[12] This has also been extended to dinuclear systems involving main-group elements, including Te[13] and Sb,[14] as well as mononuclear systems based on Ni[15] and Pt (Chart 1).[16,17] Photoelimination of HOCl and HOOOH from mononuclear Pt complexes has also been reported.[18,19]

Tellurium-containing π-conjugated molecules and polymers are semiconducting materials that can be used for organic photovoltaics and organic field-effect transistors[20−31] and as solution and solid-state phosphors.[32−40] The metalloid nature of tellurium necessitates the development of new synthetic pathways to access novel tellurium-containing heterocycles. Some recent examples include Te−B heterocycles,[41−43] 1,4-diphenyl-1-telluro-1,3-butadiene incorporated in a dibenzobarrelene skeleton,[39] a silylated oxatelluronium halide (a five-membered heterocycle containing a Te−O bond),[44] and mercaptobenzotellurazoles,[45] to name a few.

Fundamental studies of the reactivity of tellurium-containing compounds are important for the discovery of new useful transformations utilizing these compounds. Te(II)/Te(IV) redox chemistry with halogens and other oxidants has been known for quite some time. Three-center−four-electron X−Te−X bonds are formed in the presence of dihalogens or dihalogen sources where the Te(IV) atom is hypervalent (Chart 2).[20,46−51] This leads to significant changes in the optoelectronic properties of the compound. Te(II) can also be oxidized to the telluroxide or tellurone using hydrogen peroxide or organic peroxides such as *m*-chloroperoxybenzoic acid (*m*CPBA) (Chart 2).[38,39,52] In some cases, this oxidative chemistry is thermally or electrochemically reversible. Recently,

Received: November 11, 2015
Published: February 7, 2016

DOI: 10.1021/jacs.5b11649
J. Am. Chem. Soc. 2016, 138, 2678−2689

Chart 1. Transition Metal Complexes and Tellurium-Containing Compounds That Undergo Halogen Photoelimination[a]

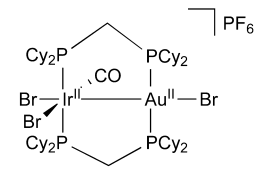

$\Phi_{320\ nm}$ = 9.4%, 2.2 M DMBD

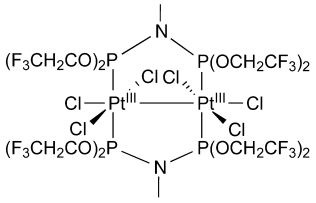

$\Phi_{510\ nm}$ = 38%, 7 M DMBD

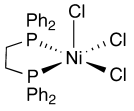

$\Phi_{370\ nm}$ = 77%, trap-free

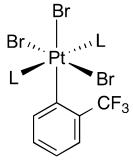

$\Phi_{313\ nm}$ = 82%, 0.13 M 1-hexene

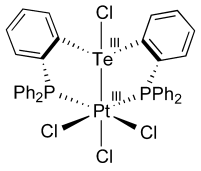

$\Phi_{350\ nm}$ = 4.4%, 2 M DMBD

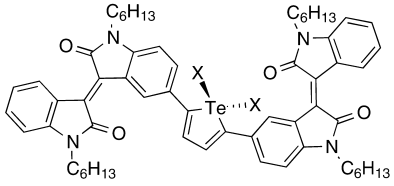

$\Phi_{505\ nm}$ = 0.2%, 2 M DMBD (X = Br, Cl)

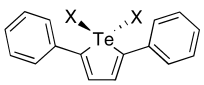

$\Phi_{447\ nm}$ = 17%, 5M DMBD (X = Br)
$\Phi_{447\ nm}$ = 1.6%, 2M DMBD (X = Cl)
$\Phi_{405\ nm}$ = 2.3%, 2M DMBD (X = F)

[a]Photoelimination quantum yields and halogen traps are indicated below the structures. DMBD = 2,3-dimethyl-1,3-butadiene.

Chart 2. Tellurium-Containing Heterocycles Prepared with Different Oxidants

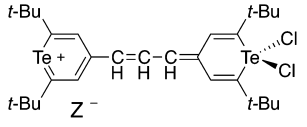

Oxidant: Cl_2

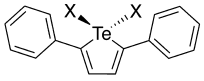

X = Br, Cl, F

Oxidant: Br_2, $PhICl_2$ or ICl, XeF_2

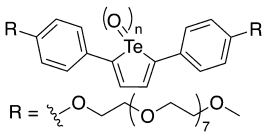

Oxidant: n = 1: H_2O_2 or *m*CPBA
n = 2: excess H_2O_2 or *m*CPBA

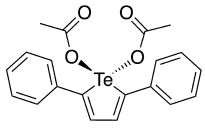

Oxidant: $PhI(OAc)_2$

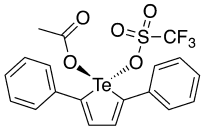

Oxidant: PhI(OAc)(OTf)

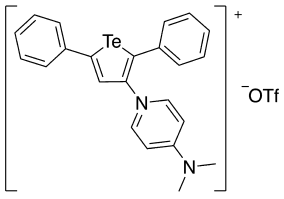

Oxidant: $PhI(4\text{-}DMAP)_2^{2+}$
Unexpected metathesis reaction

Chart 3. Chemical Structures of PT Derivatives

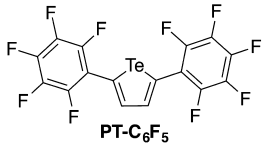

PT-C_6F_5

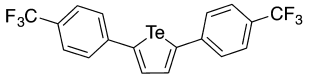

PT-CF_3

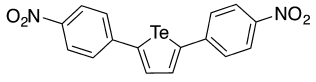

PT-NO_2

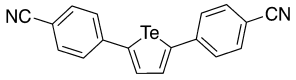

PT-CN

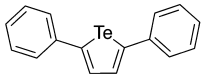

PT

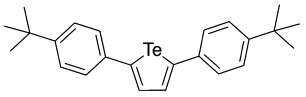

PT-*t*Bu

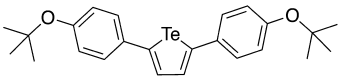

PT-O*t*Bu

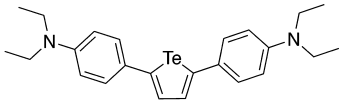

PT-NEt_2

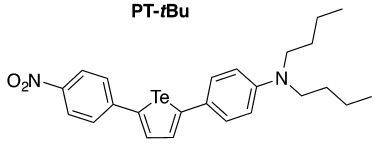

PT-NO_2-NBu_2

Dutton and co-workers reported the oxidation of 2,5-diphenyltellurophene by other iodine-based oxidants such as $PhI(OTf)_2$ and PhI(OTf)(OAc), yielding the diacetate-ligated and mixed acetate/triflate-ligated tellurophenes, respectively.[53] A rather unexpected C−H to C−N bond metathesis reaction was discovered when an analogous iodobenzene complex bearing two 4-dimethylaminopyridine (DMAP) groups was used as the oxidant, resulting in DMAP functionalization at the 3 position of the tellurophene ring (Chart 2).

We recently discovered that visible light can drive the photoreduction of Te(IV) within π-conjugated tellurophenes. The conjugated nature of the tellurophene allows the use of

DOI: 10.1021/jacs.5b11649
J. Am. Chem. Soc. 2016, 138, 2678−2689

Scheme 1. (a–c) Synthetic Routes for the Preparation of PT-R Compounds; (d) Preparation of PT-R-Br_2 Compounds

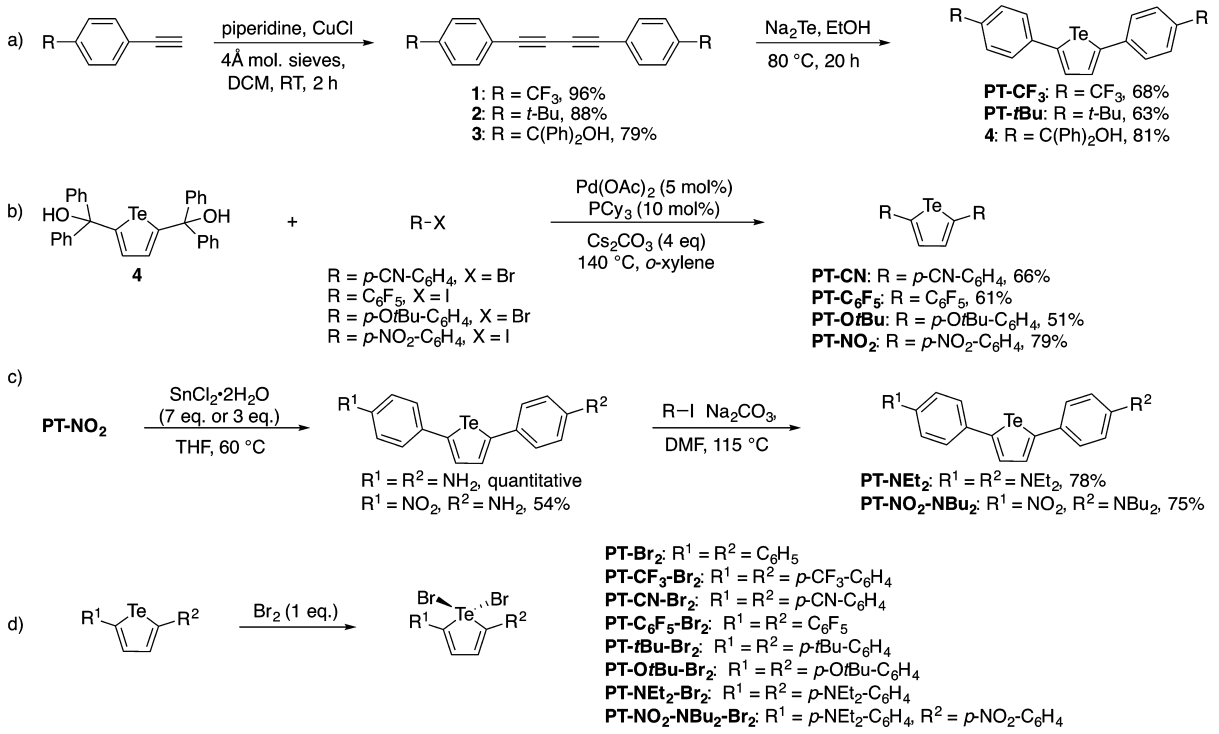

visible light to drive the reactivity. Furthermore, the ease of tunability of the substituents at the 2 and 5 positions allows tailoring of the optical properties and hence the irradiation wavelength. We previously showed that irradiation with green light can induce photoelimination of bromine and chlorine from isoindigo-functionalized tellurophenes (Chart 1), but the photochemical quantum yields of this system were limited because of unfavorable excited-state electronics.[50] Earlier this year we reported an 85-fold improvement in the quantum efficiency (up to 17%) for 2,5-diphenyltellurophene (Chart 1).[51] However, the mechanism of this reaction and its optimization are still unresolved. Here we report a series of substituted diphenyltellurophenes, focusing on the effect of electron-donating groups (EDGs) and electron-withdrawing groups (EWGs) on the structure, properties, and photochemistry of these compounds. We provide mechanistic studies of both the oxidative addition and photoelimination reactions through the use of density functional theory calculations and halogen-trapping and laser flash photolysis experiments. The optimized structures have photochemical quantum yields that exceed 40%, do not contain transition metals, and undergo photoelimination solely from the Te(IV) center.

2. RESULTS AND DISCUSSION

2.1. Molecule Design and Synthesis. 2,5-Diphenyltellurophenes can be modified with a range of functional groups to give diphenyltellurophene (**PT-R**) compounds with varying degrees of electron-donating or electron-withdrawing character (Chart 3). The electron-withdrawing substituents chosen were 4-trifluoromethylphenyl (**PT-CF_3**), 4-cyanophenyl (**PT-CN**), and pentafluorophenyl (**PT-C_6F_5**) groups. The electron-donating substituents chosen were 4-*tert*-butylphenyl (**PT-*t*Bu**), 4-*tert*-butoxyphenyl (**PT-O*t*Bu**), and 4-(*N*,*N*-diethylamino)phenyl (**PT-NEt_2**) groups. We also chose to study an asymmetric push–pull-type tellurophene bearing both an electron-donating 4-(*N*,*N*-dibutylamino)phenyl group and an electron-withdrawing 4-nitrophenyl group (**PT-NO_2-NBu_2**).

The compounds were synthesized by one of two routes: a Glaser–Hay alkyne coupling/ring-closing procedure (Scheme 1a)[54,55] or ipso-arylative cross-coupling (Scheme 1b).[56,57] The alkyne coupling/ring-closing procedure involved copper-catalyzed homocoupling of substituted terminal alkynes to form the disubstituted diacetylene precursor (compound **1** or **2**), which was then introduced into a suspension of sodium telluride (generated by reduction of tellurium powder with sodium borohydride) to give the ring-closed tellurophene product. This procedure worked well for **PT**, **PT-CF_3**, and **PT-*t*Bu**, but it was less successful for some of the other compounds, such as **PT-NEt_2**, and **PT-NO_2**, because of poor yield, poor solubility, or decomposition or because the alkyne starting material was not commercially available. Recently, Grubbs and co-workers reported that palladium-catalyzed ipso-arylation chemistry can be used to couple aryl substituents onto tellurophenes and benzotellurophenes to give polymers and small molecules.[25,26] We adopted this chemistry to synthesize the remaining tellurophene compounds. However, the previously reported synthesis of the tellurophene ipso-arylation coupling partner, 2,5-bis[(diphenyl)hydroxymethyl]-tellurophene (**4**), was modified in our study. Specifically, the diacetylene precursor **3** was synthesized via homocoupling of the commercially available alkyne, 1,1-diphenyl-2-propyn-1-ol, and then subjected to the ring-closing conditions discussed earlier to produce **4**. The tellurophene compounds **PT-O*t*Bu**, **PT-CN**, and **PT-C_6F_5** were then synthesized via ipso-arylation cross-coupling of **4** with the appropriate aryl bromide or iodide. Unfortunately, the ipso-arylation approach was also unsuccessful for the direct synthesis of **PT-NEt_2** and **PT-NO_2-NBu_2**. In order to synthesize these compounds, **PT-NO_2** was prepared via ipso-arylation followed by reduction of one or both of the

DOI: 10.1021/jacs.5b11649
J. Am. Chem. Soc. 2016, 138, 2678–2689

Table 1. Optical Absorption Properties of the Tellurophene Compounds in $CHCl_3$

	λ_{max} (nm)		ε (M^{-1} cm^{-1})			
	parent	+Br_2	parent	+Br_2	$\Delta\lambda_{max}$ (nm)	$\Delta\varepsilon$ (M^{-1} cm^{-1})
PT-NEt_2	408[a]	564[a]	3.31×10^4	1.52×10^4	156	-1.79×10^4
PT-O*t*Bu	354	465	2.56×10^4	9.70×10^3	111	-1.59×10^4
PT-*t*Bu	349	452	2.33×10^4	8.54×10^3	103	-1.48×10^4
PT	342	433	2.24×10^4	6.34×10^3	91	-1.61×10^4
PT-CN	365	417	3.12×10^4	1.11×10^4	52	-2.01×10^4
PT-CF_3	346	415	2.13×10^4	6.96×10^3	69	-1.43×10^4
PT-C_6F_5	330	408	2.52×10^4	9.29×10^3	78	-1.59×10^4
PT-NO_2-NBu_2	477[a]	566[a]	2.61×10^4	2.06×10^4	89	-5.50×10^3

[a]Measured in toluene.

nitro groups and subsequent *N*-alkyl substitution using the appropriate alkyl iodide (Scheme 1c).

2.2. Optical Properties of PT-R Compounds and Their Te(IV) Adducts. Aside from **PT-NEt_2** and **PT-NO_2-NBu_2**, all of the tellurophene compounds have similar optical absorption maxima (λ_{max}) ranging from 330 to 365 nm in chloroform with ~10^4 M^{-1} cm^{-1} molar absorptivity (Table 1). The optical absorption maxima of **PT-NEt_2** and **PT-NO_2-NBu_2** appear at longer wavelengths (408 and 466 nm, respectively, in toluene). The relatively low energy absorption of **PT-NO_2-NBu_2** is characteristic of push−pull-type chromophores. Oxidative addition of bromine to the tellurium center leads to a lower-energy λ_{max} for all of the compounds. Increasing titration with Br_2 in $CHCl_3$ (or toluene for **PT-NEt_2-Br_2** and **PT-NO_2-NBu_2-Br_2**) leads to a decrease in the absorption corresponding to the parent tellurophene accompanied by an increase in absorption at both higher- and lower-energy wavelengths (Figure 1 and Figure S1 in the Supporting Information). Clear isosbestic points (IPs) indicate clean conversion to the brominated compounds. The red shift in the lower-energy λ_{max} of the brominated compound relative to that of the parent compound is much more pronounced for compounds bearing EDGs (103, 111, and 156 nm for **PT-*t*Bu-Br_2**, **PT-O*t*Bu-Br_2**, and **PT-NEt_2-Br_2**, respectively) than those bearing EWGs (52, 68, and 78 nm for **PT-CN-Br_2**, **PT-CF_3-Br_2**, and **PT-C_6F_5-Br_2**, respectively). A red shift of 100 nm is observed for **PT-NO_2-NBu_2-Br_2**. NMR spectroscopy experiments were carried out with each tellurophene compound in $CDCl_3$ (or deuterated toluene for **PT-NEt_2** and **PT-NO_2-NBu_2**). In each case, complete conversion to the brominated product was achieved using 1 equiv of Br_2. The brominated compounds (**PT-R-Br_2**) were also synthesized on a preparative scale and isolated (Scheme 1d; see the Experimental Section in the Supporting Information for details). Additionally, the structures of **PT-*t*Bu-Br_2**, **PT-O*t*Bu-Br_2**, **PT-CF_3-Br_2**, and **PT-C_6F_5-Br_2** were confirmed by X-ray crystallography (Figure 2).

2.3. Computational Modeling. *2.3.1. Excited-State Properties.* Time-dependent density functional theory (DFT) calculations were carried out on the optimized gas-phase structures to determine the calculated absorption spectrum of each compound and the nature of the associated transitions. In general, the calculations predict the absorption spectra quite well in terms of shape and magnitude of the extinction coefficient, but the calculated spectra are overall red-shifted relative to the experimental spectra (Figure S2 in the Supporting Information). For all of the compounds (including the brominated compounds), the lowest-energy transition with significant oscillator strength is HOMO-to-LUMO in nature. The calculations predict a decreased HOMO−LUMO energy gap upon bromination (Figure S3 in the Supporting Information) that is consistent with the experimental spectra. Visualization of the frontier molecular orbitals (MOs) of the non-brominated tellurophenes show that this transition is a delocalized $\pi-\pi^*$ transition, while the HOMO-to-LUMO transition in the brominated compounds has charge-transfer character from a delocalized state onto the dibromotellurophene unit (Figure 3). The LUMO has significant electron density within the antibonding Te−Br orbitals. Excitation into this state should promote photoelimination of bromine.

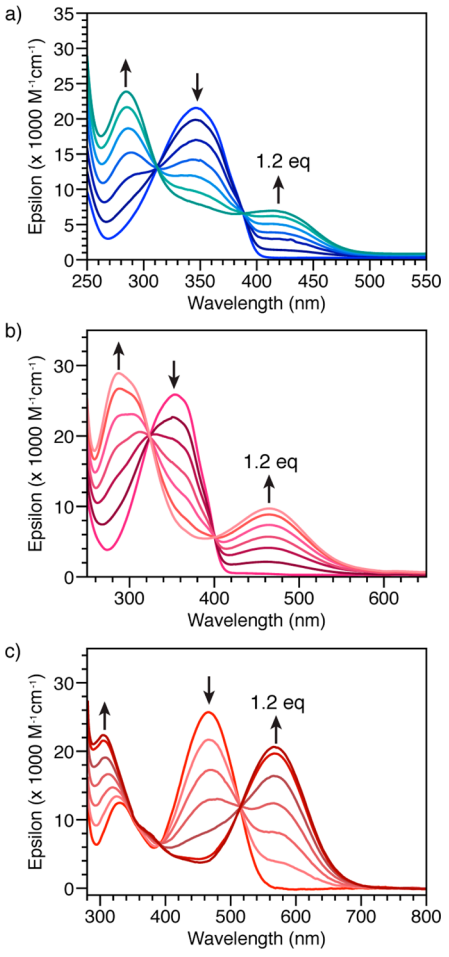

Figure 1. Optical absorption spectra of bromine titration experiments for (a) **PT-CF_3** ($CHCl_3$), (b) **PT-O*t*Bu**, ($CHCl_3$), and (c) **PT-NO_2-NBu_2** (toluene).

2.3.2. Oxidative Addition Mechanistic Study. It is important to note that the mechanism of bromine addition

DOI: 10.1021/jacs.5b11649
J. Am. Chem. Soc. 2016, 138, 2678−2689

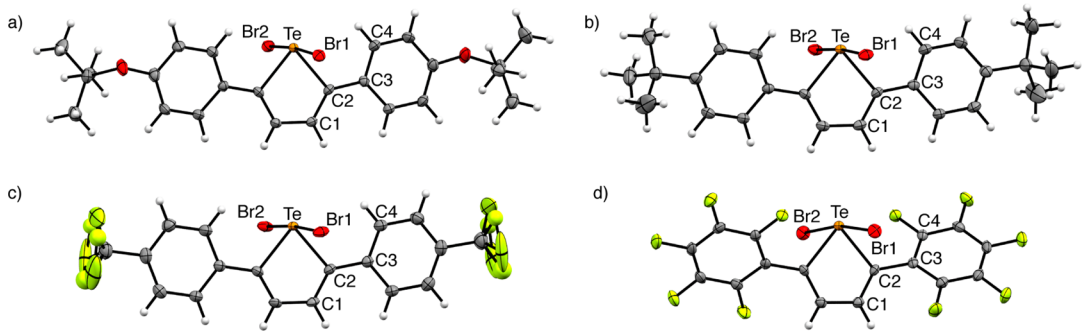

Figure 2. Displacement ellipsoid plots of (a) **PT-O*t*Bu-Br$_2$**, (b) **PT-*t*Bu-Br$_2$**, (c) **PT-CF$_3$-Br$_2$** (the F atoms are disordered over two sets of sites; the minor component is shown as small spheres), and (d) **PT-C$_6$F$_5$-Br$_2$** shown at 50% probability.

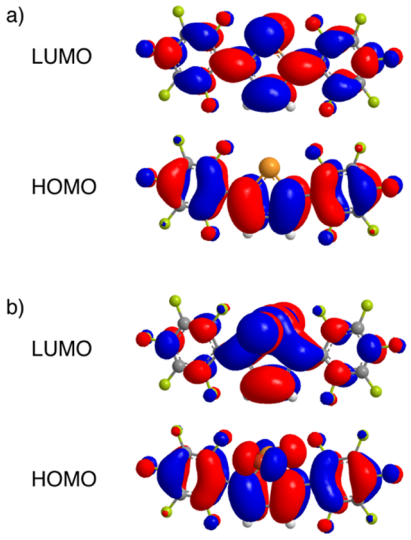

Figure 3. Molecular orbital diagrams for (a) **PT-C$_6$F$_5$** and (b) **PT-C$_6$F$_5$-Br$_2$**.

to tellurophene is unknown. Detty and co-workers proposed two possible mechanisms for this reaction involving other organotellurium compounds.[48] Stopped-flow kinetics experiments revealed three distinct processes: an initial "fast" reaction followed by two slower ones. The "fast" reaction was attributed to the formation of an initial association complex between molecular bromine and the tellurium atom, which was speculated to have either an "end-on" η^1 or "edge-on" η^2 geometry. From here, the addition of Br_2 to tellurium could occur via either a concerted mechanism (from an η^2 association complex; Scheme 2a) or a dissociative mechanism (from an η^1 association complex) with the formation of an ionic intermediate (Scheme 2b).

Here we used DFT geometry optimizations to model molecular bromine in close proximity to diphenyltellurophene. Three different minima were found depending on the starting positions of the molecules in the input file. One structure resembles an "end-on" η^1 association complex (**Int1**), another resembles a monobrominated species suggestive of an ionic intermediate (**Int2**), and the last structure resembles that of the brominated product (**PT-Br$_2$**). Frequency calculations verified that each of these structures is a minimum. Attempts to locate an optimized structure involving an "edge-on" η^2 association complex were unsuccessful.

Synchronous transit-guided quasi-Newton[58,59] (STQN) calculations were performed to locate a transition state

Scheme 2. Possible Mechanisms for Oxidative Addition of Molecular Bromine to Organotellurium Compounds: (a) Concerted Mechanism Involving an η^2 Association Complex; (b) Dissociative Mechanism Involving an η^1 Association Complex and an Ionic Intermediate[a]

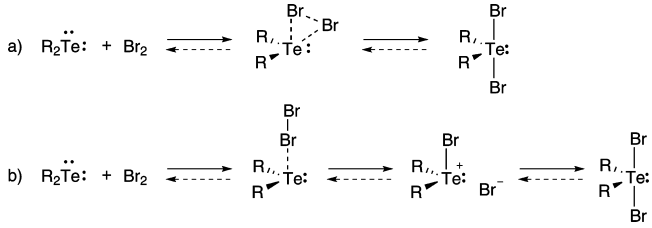

[a]Adapted and simplified from ref 48.

connecting **Int1** with **Int2** (**TS1-2**) and another connecting **Int2** with **PT-Br$_2$** (**TS2-P**). The transition-state calculations were successfully optimized to maxima, resulting in structures with geometries intermediate between those of the two minima that they connect. To verify that **TS1-2** and **TS2-P** are the true transition-state structures, frequency calculations and intrinsic reaction coordinate (IRC)[60] calculations were performed. The frequency calculations predicted one negative frequency, which is expected for a transition state. The vibrations associated with this negative frequency involve motions of the bromine atoms in a manner that supports a transition from **Int1** to **Int2** in the case of **TS1-2** and from **Int2** to **PT-Br$_2$** in the case of **TS2-P**. IRC calculations follow the reaction pathway from the transition state to the minima and can confirm whether a calculated transition-state structure truly connects the two minima of interest. IRC calculations from **TS1-2** and from **TS2-P** indeed led to structures resembling **Int1**, **Int2**, and **PT-Br$_2$** as expected (Figures S4 and S5 in the Supporting Information), and geometry optimizations starting from the final IRC structures led to the identical minimum-energy structures that were obtained from the geometry optimizations of Br_2 in close proximity to **PT** discussed earlier.

Although attempts to locate a minimum-energy η^2 association complex were unsuccessful, attempts were also made to locate a transition state with this structure. A maximum was successfully located, but the molecular distortion associated with the negative frequency does not involve the bromine atoms and thus does not support a connection to the product structure. Furthermore, IRC calculations from this structure were unsuccessful. Thus, no evidence for a concerted oxidative addition mechanism was found. Finally, an attempt to connect **Int1** directly to **PT-Br$_2$** through a single transition

DOI: 10.1021/jacs.5b11649
J. Am. Chem. Soc. 2016, 138, 2678−2689

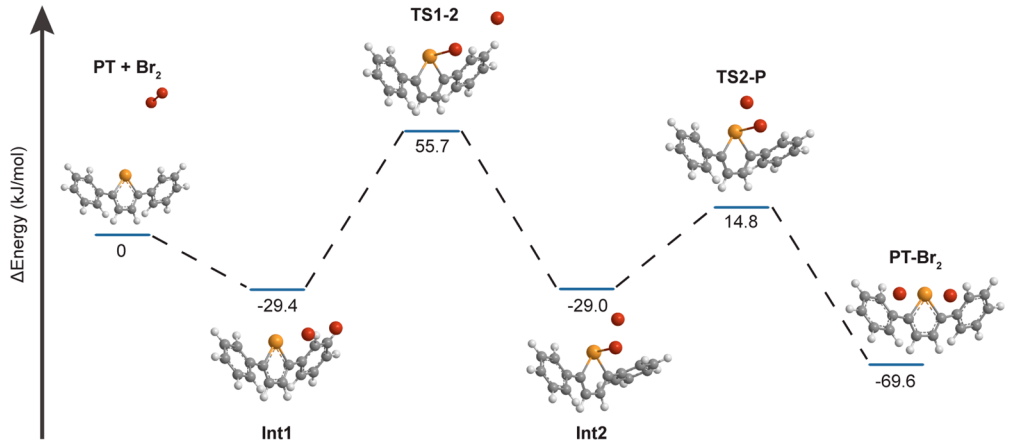

Figure 4. DFT-calculated reaction pathway energy diagram for the oxidative addition of bromine to **PT**, calculated with a $CHCl_3$ PCM.

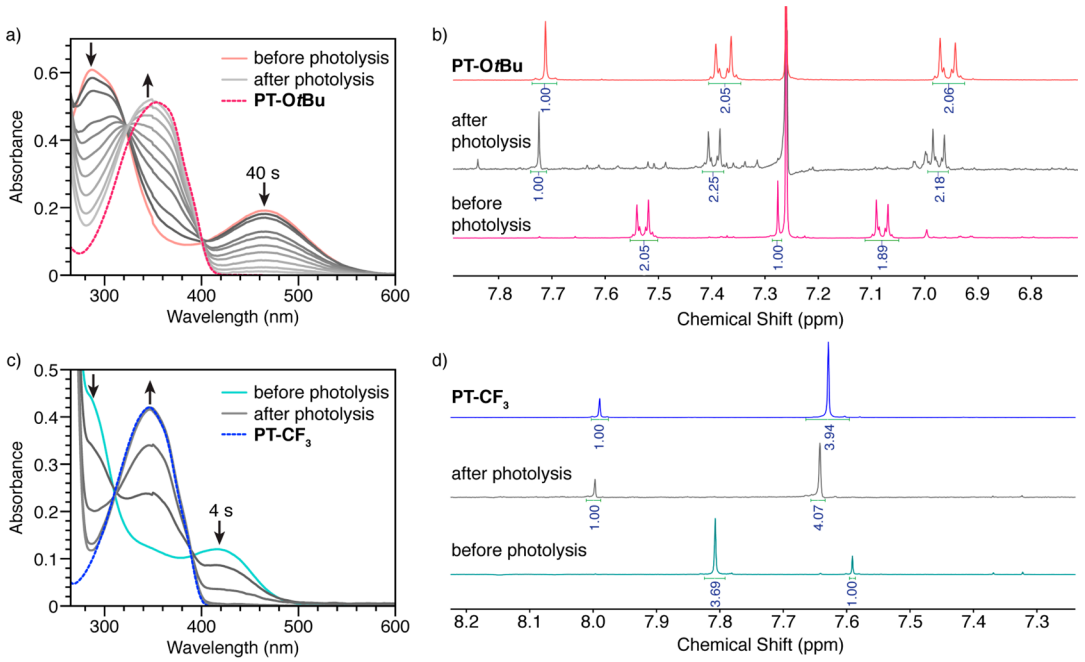

Figure 5. Optical absorption and ^{1}H NMR spectra showing the photolysis of (a, b) **PT-O*t*Bu-Br$_2$** and (c, d) **PT-CF$_3$-Br$_2$**.

state was also made. The calculation successfully optimized to a maximum structure, but this structure was identical to **TS1-2**, and the IRC calculation led to structures resembling **Int1** and **Int2** rather than **PT-Br$_2$**. This confirms that **TS1-2** does not connect **Int1** directly to the product (**PT-Br$_2$**) but instead connects it to the monobrominated intermediate **Int2**. Overall, the results of the DFT calculations support a three-step oxidative addition mechanism involving the sequential formation of an initial η^1 association complex, a monobrominated intermediate, and finally the brominated product (Scheme 2b).

Scaled frequency calculations and high-accuracy single-point energy calculations were performed for all of the optimized structures in order to determine accurate zero-point-corrected energies. The calculations were also repeated using a chloroform polarizable continuum model (PCM). The geometries obtained with the chloroform model are only slightly different than the gas-phase geometries. The zero-point-corrected energies obtained from the calculations with the solvent model were used to produce a reaction pathway energy diagram for the oxidative addition process (Figure 4). Although the geometries calculated with the solvent model are similar to the optimized gas-phase geometries, the energies of all structures are stabilized when the chloroform model is applied. A much larger degree of stabilization is predicted for the monobrominated intermediate **Int2** and the transition states connecting **Int2** to its reactant and product (Figure S6 in the Supporting Information).

2.4. Photochemistry. *2.4.1. Photolysis Experiments.* Photolysis experiments were carried out on the brominated compounds by irradiation at the lowest-energy absorption band. The reactions were monitored using optical absorption spectroscopy. We will first discuss **PT-Br$_2$** and the compounds bearing EDGs. Irradiation of **PT-Br$_2$**, **PT-*t*Bu-Br$_2$**, and **PT-O*t*Bu-Br$_2$** at 447 nm in the presence of 1 M 2,3-dimethyl-1,3-butadiene (DMBD), a halogen trap, led to spectral changes consistent with conversion back to the parent compounds. A comparison of the photolysis product spectra with those of each of the parent compounds showed some differences, specifically a slight blue shift in both λ_{max} and the isosbestic

DOI: 10.1021/jacs.5b11649
J. Am. Chem. Soc. 2016, 138, 2678−2689

points (Figure S7 in the Supporting Information). This is attributed to the formation of decomposition products during photolysis. On the basis of the magnitude of the difference between the photolysis product spectrum and the parent spectrum, the amount of decomposition is more significant for compounds with stronger EDGs. Increasing the DMBD concentration to 3 M, however, leads to clean conversion of **PT-Br$_2$** to **PT** and only slight decomposition in the cases of **PT-*t*Bu-Br$_2$** (Figure S8 in the Supporting Information) and **PT-O*t*Bu-Br$_2$** (Figure 5a). Photolysis was complete within 5, 16, and 40 s for **PT-Br$_2$**, **PT-*t*Bu-Br$_2$**, and **PT-O*t*Bu-Br$_2$**, respectively, showing that the irradiation time required to achieve complete conversion increases with donating strength. This is consistent with strong electron-donating character hindering the reductive elimination process. Because of the low-energy absorption of **PT-NEt$_2$-Br$_2$** and **PT-NO$_2$-NBu$_2$-Br$_2$**, red-orange (617 nm) light was used for irradiation. For the strongly donating **PT-NEt$_2$-Br$_2$**, photolysis was complete within 6 min and the optical absorption spectrum is indicative of the formation of decomposition products (Figure S8 in the Supporting Information), consistent with the results for the other compounds bearing EDGs. Interestingly, a much longer irradiation time was required for **PT-NO$_2$-NBu$_2$-Br$_2$** (160 min), and the optical absorption spectrum indicates an even greater amount of decomposition, as evidenced by the blue-shifted λ_{max} and isosbestic points.

We next discuss the compounds bearing EWGs. Irradiation of **PT-CF$_3$-Br$_2$** (Figure 5c), **PT-CN-Br$_2$**, and **PT-C$_6$F$_5$-Br$_2$** (Figure S8 in the Supporting Information) at 430 nm in the presence of 3 M DMBD led to complete conversion back to the respective parent compounds within a few seconds. For these compounds, the optical absorption spectra of the photolysis products are identical to the spectra of the parent compounds, and there is no evidence of decomposition.

All of the photolysis reactions were also characterized by NMR spectroscopy. Consistent with the optical absorption spectra, some decomposition was observed during the photolysis of **PT-*t*Bu-Br$_2$** (Figure S9 in the Supporting Information) and **PT-O*t*Bu-Br$_2$** (Figure 5b), as indicated by the presence of additional peaks in the aromatic region as well as some discrepancy in the integration of the tellurophene proton signals. Photolysis of **PT-NEt$_2$-Br$_2$** and **PT-NO$_2$-NBu$_2$-Br$_2$** leads to decomposition, and no evidence of the brominated starting materials could be seen (Figures S10 and S11 in the Supporting Information). On the other hand, photolysis of **PT-CF$_3$-Br$_2$** (Figure 5d), **PT-C$_6$F$_5$-Br$_2$**, and **PT-CN-Br$_2$** (Figures S12 and S13 in the Supporting Information) leads to complete conversion to the parent compounds with no evidence of additional product formation in the NMR spectra, confirming that these reactions are quite efficient and free of side reactions. The tellurophene compounds demonstrate high thermal stability, and thus, thermal reduction is of no concern in the photolysis experiments (see the Supporting Information for thermal control experiments).

2.4.2. Photochemical Quantum Yield Determination. The efficiencies of photoelimination were evaluated by determining the photochemical quantum yield, Φ_p, using potassium ferrioxalate actinometry (Table 2).[61−63] **PT-Br$_2$** has a photochemical quantum yield of 8.5% at a DMBD concentration of 2 M.[51] The incorporation of EDGs onto the phenyl ring reduces the photoelimination quantum yield for **PT-*t*Bu-Br$_2$** (1.61 ± 0.04%) and **PT-O*t*Bu-Br$_2$** (0.44 ± 0.01%). On the contrary, the incorporation of EWGs increases the quantum yield for **PT-CN-Br$_2$** (14.7 ± 0.3%), **PT-CF$_3$-Br$_2$** (19.2 ± 0.7%), and **PT-C$_6$F$_5$-Br$_2$** (23.6 ± 0.7%). These observations are consistent with the EWGs facilitating photoelimination by making Te more electropositive.

Table 2. Photochemical Quantum Yields for Photoelimination of Bromine from PT Derivatives

	[DMBD] (M)	Φ_p (%)[a]	std. dev. (%)	relative Φ_p
PT-NEt$_2$-Br$_2$	2	–	–	0.007[b]
PT-O*t*Bu-Br$_2$	2	0.44	0.01	0.05
PT-*t*Bu-Br$_2$	2	1.61	0.04	0.2
PT-Br$_2$	2	8.5	0.3	1
PT-CN-Br$_2$	2	14.7	0.3	1.7
PT-CF$_3$-Br$_2$	2	19.2	0.7	2.3
PT-C$_6$F$_5$-Br$_2$	1	17.6	0.5	
	2	23.6	0.7	2.8
	3	31.3	0.2	
	4	36.6	0.5	
	5	42.4	0.4	
PT-NO$_2$-NBu$_2$-Br$_2$	2	–	–	0.0002[b]

[a]Determined by potassium ferrioxalate actinometry. [b]Estimated from the output of the light source and the change in concentration for a given irradiation period.

The quantum yields for **PT-NEt$_2$-Br$_2$** and **PT-NO$_2$-NBu$_2$-Br$_2$** could not be determined since the irradiation wavelength (617 nm) was beyond the absorption range of the actinometer. However, the radiant power of the light sources (from manufacturer specifications) and the change in concentration for a given irradiation period were considered in order to draw a relative comparison (see the Supporting Information for the detailed calculations). From these calculations, bromine photoelimination from **PT-NEt$_2$-Br$_2$** and **PT-NO$_2$-NBu$_2$-Br$_2$** is approximately 0.007 and 0.0002 times less efficient, respectively, than that from **PT-Br$_2$** (Table 2).

The extremely poor efficiency for **PT-NO$_2$-NBu$_2$-Br$_2$** is somewhat surprising. It might be expected that **PT-NO$_2$-NBu$_2$-Br$_2$** would have photochemical behavior similar to that of unsubstituted **PT-Br$_2$** as a result of a canceling effect of the strong EDG and EWG at either end of the molecule. Rationalization of the unprecedented low efficiency was attempted on the basis of electrostatic potential (ESP) maps from the DFT calculations. The ESP maps of **PT-Br$_2$**, **PT-NEt$_2$-Br$_2$**, and **PT-C$_6$F$_5$-Br$_2$** show increasing positive ESP at Te with increasing electron-withdrawing character (Figure 6a). The incorporation of both a strong EWG at one end and a strong EDG at the other end of the molecule does indeed have a canceling effect on the ESP at Te, resulting in an ESP map for **PT-NO$_2$-NBu$_2$-Br$_2$** that is quite similar to that of **PT-Br$_2$**. Thus, the sluggish photochemical behavior cannot be explained by an ESP argument. Instead, analysis of the MO diagrams provides more insight into this behavior. The MO diagrams for **PT-NO$_2$-NBu$_2$-Br$_2$** display the typical charge-transfer character of push−pull chromophores. Thus, rather than being localized only on the dibromotellurophene ring, as is the case for the other derivatives, the electron density in the LUMO is delocalized across both the dibromotellurophene ring and the NO$_2$-substituted phenyl ring (Figure 6b). This decreases the Te−Br antibonding character in the LUMO compared with the other derivatives, which likely explains the unexpected poor efficiency observed for this compound.

DOI: 10.1021/jacs.5b11649
J. Am. Chem. Soc. 2016, 138, 2678−2689

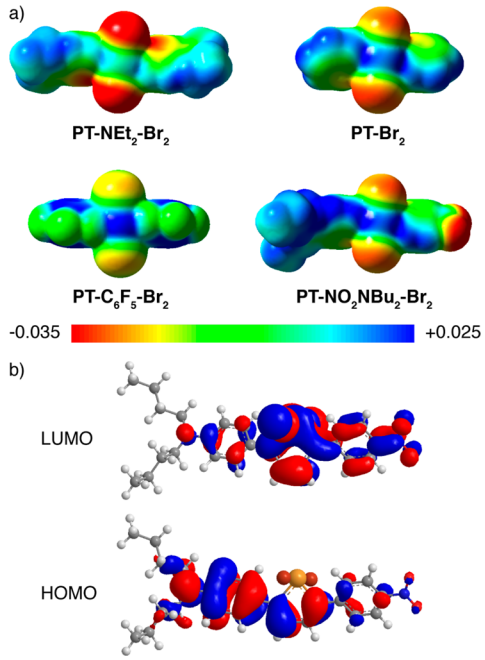

Figure 6. (a) ESP maps of the indicated compounds. (b) MO diagrams for **PT-NO_2-NBu_2-Br_2**.

Finally, a trap-dependent quantum yield study was carried out for the most efficient compound, **PT-C_6F_5-Br_2** (Table 2). A linear dependence of the quantum yield on the trap concentration was observed (Figure S14 in the Supporting Information), with an impressive value of 42.4 ± 0.4% at a DMBD concentration of 5 M, the best value for a tellurophene reported to date.

2.5. Mechanistic Details of Tellurophene Photochemistry. *2.5.1. Halogen Trapping Experiments.* To gain insight into the photoelimination mechanism, the identity of the liberated bromine species was investigated by characterizing the trapped products. For these experiments, **PT-C_6F_5-Br_2** was the reactant and 2,3-dimethyl-2-butene (DMB) was used as the trap in order to reduce the number of possible trap products. Molecular bromine would be expected to yield the Br_2 addition product 2,3-dibromo-2,3-dimethylbutane (DMB-Br_2).[64] Thus, if bromine is reductively eliminated as Br_2 (or leads to the formation of Br_2), this would be the only expected trap product. On the other hand, if bromine is released as two bromine radicals ($Br^{\bullet}$), then reaction of one $Br^{\bullet}$ with DMB would be expected to yield HBr and an allylic radical ($DMB^{\bullet}$), which could then react with the second $Br^{\bullet}$ to produce 1-bromo-2,3-dimethyl-2-butene (DMB-Br).[65] Additionally, the HBr produced from this process could also react with DMB to give the HBr addition product 2-bromo-2,3-dimethylbutane (DMB-HBr).[66] Evidence of both the allylic bromination product DMB-Br (singlet at δ = 4.08 ppm) and the Br_2 addition product DMB-Br_2 (singlet at δ = 2.03 ppm) are present after photolysis (Figure S15a in the Supporting Information). The ratio of DMB-Br to DMB-Br_2 is approximately 6:1, suggesting that the dominant pathway involves $Br^{\bullet}$. Compared to the integration of **PT-C_6F_5**, the yields are 39% DMB-Br and 7% DMB-Br_2, which suggests that 54% of the liberated bromine is consumed in additional processes. Surprisingly, there is no evidence of DMB-HBr in the ^{1}H NMR spectrum, despite the fact that DMB-Br is formed in 39% yield. However, after photolysis there are several other significant peaks in the alkyl region with unknown identities (singlets at δ = 1.93, 1.86, 1.85, and 1.49 ppm; Figure S15b in the Supporting Information), which could account for the remaining trapped bromine.

In order to further investigate bromine trapping, GC−MS analysis was carried out on the photolyzed samples. The trapped products DMB-Br_2 and DMB-Br were prepared separately for comparison (Figures S16 and S17 in the Supporting Information). Evidence of both DMB-Br_2 (retention time = 6.05 min) and DMB-Br (retention time = 4.94 min) was observed in the photolyzed sample (Figure S18 in the Supporting Information). However, additional product(s) with a retention time of 4.92 min coeluted with DMB-Br. An analysis of the chromatogram peak at 4.94 min shows the expected mass for DMB-Br, with two equal-intensity peaks at m/z 162 and 164. Analysis of the same chromatogram peak at 4.92 min also shows two peaks of roughly equal intensity in the MS spectrum, but these are shifted to m/z 165 and 167. While the retention time and MS pattern of the unidentified product(s) are suggestive of a monobrominated alkane, extensive efforts to determine the identity of the compound(s) were unsuccessful (for further discussion, see the Supporting Information).

The expected retention time for **PT-C_6F_5** is 12.71 min, and the photolysis product exhibited only a slight difference in retention time (12.76 min) with an identical fragmentation pattern (Figure S19 in the Supporting Information). Comparison of the integration of the DMB-Br_2 peak in the GC trace with the **PT-C_6F_5** peak gives a ratio of 0.063:1, corresponding to a 6.3% yield of DMB-Br_2 (Figure S20 in the Supporting Information). This is in excellent agreement with the yield determined by NMR integration. Comparing the integration of the peak at 4.92 min (which contains both DMB-Br and the other product(s)) with that of **PT-C_6F_5** gives a ratio of 0.77:1, corresponding to a 77% yield of these products. This is roughly twice the NMR-determined yield of DMB-Br, suggesting a 1:1 ratio of DMB-Br to the unidentified trap product(s). The total yield of the discussed products from the GC analysis is approximately 83%. There are a few other low-intensity peaks in the GC trace with retention times ranging from 6.56 to 8.67 min, which likely account for the remainder of the trapped bromine.

Although the identity of the additional major trapped product(s) remains unclear, the results of the trapping experiments show that the photoelimination reaction occurs predominantly by elimination of radical bromine. The Br_2 addition product, which is formed in very small quantities, could be formed by Br_2 produced by combination of two eliminated bromine radicals (vide infra).

2.5.2. Laser Flash Photolysis Experiments. To further investigate the mechanism of the photoelimination reaction, nanosecond laser flash photolysis (LFP) experiments were performed on the compounds with the highest photochemical quantum yields, **PT-Br_2**, **PT-CN-Br_2**, **PT-CF_3-Br_2**, and **PT-C_6F_5-Br_2** (see the Supporting Information for the experimental setup and conditions). The brominated compounds were excited within the low-energy absorption band using a 450 nm excitation pulse in the presence of DMBD under an argon atmosphere. The transient absorption (TA) spectra of **PT-CF_3-Br_2** in the presence of ∼0.2 M DMBD (3000:1 trap:tellurophene ratio) recorded at different times after the laser pulse display intense absorption bands at about 360 and 325 nm (Figure 7a). Similar features were observed in the TA spectra of

DOI: 10.1021/jacs.5b11649
J. Am. Chem. Soc. 2016, 138, 2678−2689

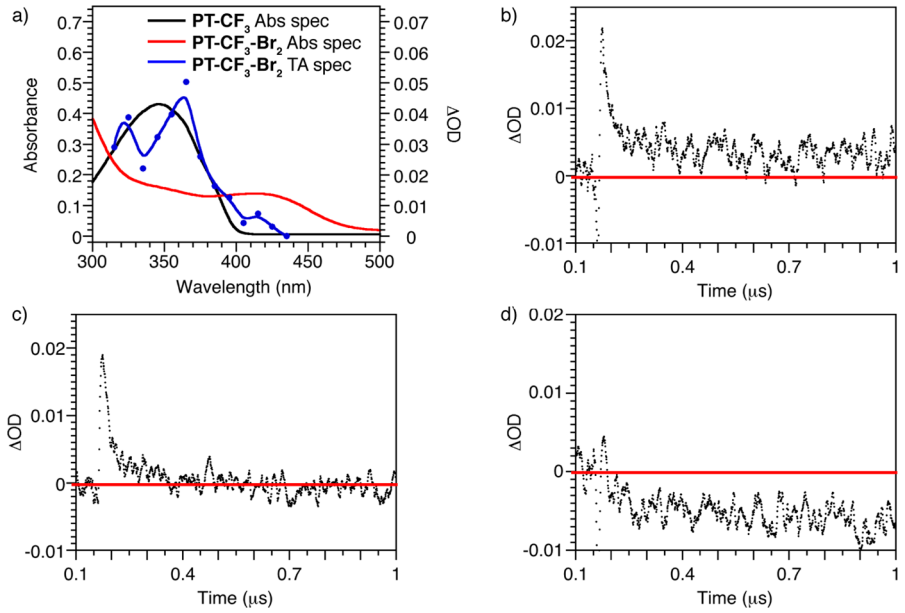

Figure 7. (a) Optical absorption spectra of **PT-CF$_3$** and **PT-CF$_3$-Br$_2$** compared with the TA spectrum of **PT-CF$_3$-Br$_2$** in the presence of DMBD right after the 450 nm laser pulse. (b–d) Single-wavelength kinetic traces of $CHCl_3$ solutions of **PT-CF$_3$-Br$_2$** excited at 450 nm and monitored at (b) 388 nm, (c) 392 nm, and (d) 430 nm.

the other three compounds (Figure S21 in the Supporting Information).

Single-wavelength kinetic traces obtained at and about the low-energy isosbestic point between the photoreactant (**PT-R-Br$_2$**) and the photoproduct (**PT-R**) were used to determine the nature of the observed transient species. Because the ground-state absorption of **PT-R** is greater than that of **PT-R-Br$_2$** at wavelengths shorter than the IP, the decay of a single-wavelength trace to a final positive ΔOD is expected, confirming conversion of **PT-R-Br$_2$** to **PT-R**. On the other hand, at wavelengths longer than the IP, **PT-R** absorbs less than **PT-R-Br$_2$**, and a final negative ΔOD is expected. At the IP, the absorbances of the photoreactant and photoproduct are equal, and thus, they are silent in LFP and a final ΔOD of zero is expected. As a result, any signal observed in the kinetics trace could be attributed to the presence of a transient species. Single-wavelength kinetic traces were collected at several wavelengths for **PT-CF$_3$-Br$_2$** (Figure 7b–d), **PT-Br$_2$**, **PT-CN-Br$_2$**, and **PT-C$_6$F$_5$-Br$_2$** (Figure S22 in the Supporting Information) in the presence of ∼0.2 M DMBD. Indeed, the ΔOD monitored at the IP decays to zero after excitation, and in all cases a transient species with positive ΔOD is formed within the pulse of the laser (5–8 ns). Since this is the only active species at the IP, the decay can be used to determine the lifetimes of the transient species, which are 20–70 ns for the different compounds (Table 3). Further discussion and a possible assignment of this transient will be presented below.

Table 3. Lifetimes of the Transient Species Generated upon 450 nm Excitation

sample	monitored wavelength (nm)	τ (ns)
PT-C$_6$F$_5$-Br$_2$ + DMBD	371	42.1–39.2
PT-CF$_3$-Br$_2$ + DMBD	390	45–42–39
PT-CN-Br$_2$ + DMBD	406	22.4–16.4–23.3
PT-Br$_2$ + DMBD	398	77.0–60.9

The IPs located by LFP are in good agreement with the IPs observed in the steady-state optical absorption photolysis experiments, with the exception of that for **PT-Br$_2$**. When the **PT-Br$_2$** sample was probed at 386 nm (the IP determined during the steady-state photolysis experiments), a final positive ΔOD was unexpectedly observed, while a final ΔOD of zero was observed when the sample was probed at 398 nm. At the trap concentration used in these experiments, it is likely that this compound undergoes some amount of decomposition, which may explain the discrepancy observed, although a blue-shifted IP is usually observed when decomposition is present.

In order to assign the observed transient species and to gain insight into the photochemical mechanism, a series of experiments were performed. First, the possibility of triplet state formation due to the presence of the heavy atom tellurium was probed. Upon excitation of the non-brominated tellurophene **PT-CF$_3$** at 355 nm, an absorption band appears at 450 nm in the TA spectrum. The lifetime of this transient species is 1.3 μs, and this band is attributed to absorption by the **PT-CF$_3$** triplet state. This is in agreement with the calculated absorption spectrum of the ground-state triplet by DFT (Figure S23 in the Supporting Information). Interestingly, the TA spectrum and lifetime observed upon excitation of **PT-CF$_3$-Br$_2$** at 355 nm are different from the TA spectrum and lifetime obtained when **PT-CF$_3$-Br$_2$** is excited at 450 nm, which suggests that different transient species are formed under the different photolysis conditions. Furthermore, the TA spectrum and lifetime (1.3 μs) for **PT-CF$_3$-Br$_2$** are similar to those obtained for **PT-CF$_3$** when excitation at 355 nm is used (Figure 8), indicating that the same transient species was observed in these two samples. Since this transient was attributed to the **PT-CF$_3$** triplet, it follows that the dehalogenation process and excitation of the photoproduct must be complete within the pulse of the laser (5–8 ns). The **PT-CF$_3$** excited-state singlet may then undergo intersystem crossing (ISC) to give the observed **PT-CF$_3$** triplet (Scheme S1 in the Supporting Information). This pathway cannot be accessed when a 450 nm laser pulse is used since the photoproduct does not absorb at this wavelength. Thus, the

DOI: 10.1021/jacs.5b11649
J. Am. Chem. Soc. 2016, 138, 2678–2689

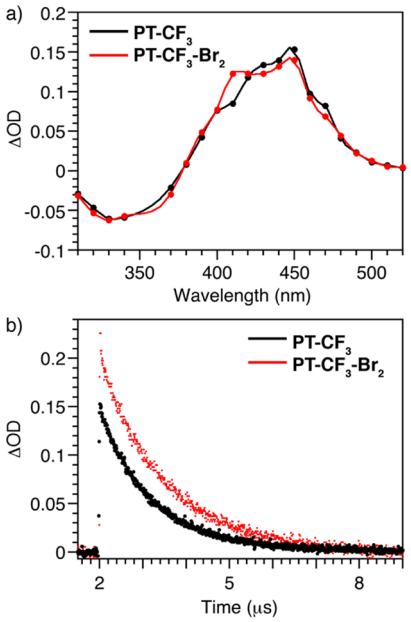

Figure 8. (a) TA spectra and (b) single-wavelength kinetic traces (monitored at 410 nm) obtained for $CHCl_3$ solutions of **PT-CF$_3$-Br$_2$** and **PT-CF$_3$** containing DMBD upon irradiation at 355 nm under an Ar atmosphere. Lifetime ≈ 1.3 μs.

transient species with a lifetime of ∼45 ns is observed under 450 nm excitation.

To further confirm the presence of triplet states, steady-state photoluminescence measurements on both **PT-CF$_3$** and **PT-CF$_3$-Br$_2$** were performed at low temperature (∼77 K) under argon (Figure S24 in the Supporting Information). A phosphorescence band at 440 nm was observed for **PT-CF$_3$** (excitation at 355 nm), and two bands around 550 and 600 nm were observed for **PT-CF$_3$-Br$_2$** (excitation at 450 nm). Additionally, under an O_2 atmosphere, both **PT-CF$_3$** and **PT-CF$_3$-Br$_2$** generate singlet oxygen ($^1O_2$) when they are excited at 355 and 450 nm, respectively. The $^1O_2$ quantum yield (Φ_Δ) approaches unity for **PT-CF$_3$** ($\Phi_\Delta \approx 1.0$) and is lower for **PT-CF$_3$-Br$_2$** ($\Phi_\Delta \approx 0.1$) in the absence of trap using *meso*-tetraphenylporphyrin (TTP) as a standard ($^{TPP}\Phi_\Delta \approx 0.66$ in CCl_4 and benzene).[67] Furthermore, **PT-CF$_3$** does not generate $^1O_2$ when irradiated at 450 nm, suggesting that both **PT-CF$_3$** and **PT-CF$_3$-Br$_2$** generate $^1O_2$ from their respective triplet states. This evidence of **PT-CF$_3$-Br$_2$** triplet state formation suggests that ISC is competitive with bromine photoelimination.

As discussed above, the halogen trapping experiments suggest that the bromine species generated upon photolysis is most likely Br$^\bullet$. However, direct detection of this species would be desired in order to fully characterize the photoelimination mechanism. Thus, it is important to identify a molecule that would react efficiently with Br$^\bullet$ to yield a readily detectable species. The reaction of bromide (Br^-) with bromine atoms (Br$^\bullet$) provides an ideal probe reaction since the product ($Br_2^{\bullet-}$) absorbs strongly at 360 nm (ε_{360} = 9000 M^{-1} cm^{-1}).[68] Kinetic traces obtained upon excitation of solutions of **PT-C$_6$F$_5$-Br$_2$** and **PT-CF$_3$-Br$_2$** in the presence of tetraethylammonium bromide (TEABr) (3 mM) show a long-lived intermediate (∼9−12 μs) when monitored at the IPs (371 and 390 nm, respectively). Since these wavelengths coincide with the absorption of $Br_2^{\bullet-}$, the transient observed can be attributed to the formation of this intermediate. To further confirm this, TA spectra were recorded within 100 ns after excitation and compared to the TA spectra obtained for the solutions containing the DMBD trap. For both **PT-CF$_3$-Br$_2$** and **PT-C$_6$F$_5$-Br$_2$**, subtraction of the two spectra reveals an absorption band centered at 385 nm, attributed to absorption by $Br_2^{\bullet-}$ (Figure 9 and Figure S25 in the Supporting Information, respectively). The same profile was found at various times after excitation. Thus, the absorption profile in the TA spectra and the long lifetimes support the formation of $Br_2^{\bullet-}$, which is further confirmation that photoelimination involves the release of bromine radicals (Scheme 3a).

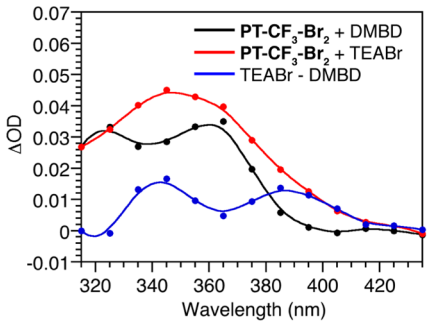

Figure 9. TA spectra of **PT-CF$_3$-Br$_2$** in the presence of DMBD and TEABr recorded within 100 ns after the laser pulse (450 nm) and the arithmetic subtraction of the two spectra.

In accordance with all of these results, plausible photochemical and photophysical mechanisms for both the nonbrominated and brominated tellurophene systems can be described (Scheme 3b,c). Upon irradiation at 450 nm, **PT-R-Br$_2$** is excited to its very short lived singlet excited state, S_1 (τ < 2 ns, no fluorescence emission detected), which is subject to either of the following competitive pathways: (a) intersystem crossing to the triplet excited state, T_1 (path 1), followed by the concomitant relaxation to the singlet ground state, S_0, via radiative relaxation (phosphorescence, ∼600 nm), nonradiative relaxation (path 2), or energy transfer to $^3O_2$ under aerobic conditions; or (b) photodebromination via stepwise Br$^\bullet$ elimination (path 3), which occurs within the time resolution of the instrument and was confirmed by detection of $Br_2^{\bullet-}$ when LFP was carried out in the presence of TEABr (absorption at 380 nm with a lifetime of ∼10 μs). The parent compounds (**PT-R**) can be excited using a 355 nm pulse and can undergo paths 1 and 2 explained above (labeled 1′ and 2′ in Scheme 3c) or generate $^1O_2$ under aerobic conditions.

Reasonable assignments for the ∼50 ns transient species observed during LFP of the brominated compounds (Table 3) could be (a) a photointermediate such as the monobrominated species **PT-R-Br**$^\bullet$ formed after the first Br$^\bullet$ elimination, (b) a singlet excited state of the photoreactant, or (c) a triplet excited state of the photoreactant. The observation of the **PT-CF$_3$** triplet state (1.3 μs lifetime) upon excitation of **PT-CF$_3$-Br$_2$** at 355 nm necessitates that dehalogenation, excitation of the photoproduct, and ISC all occur within the duration of the laser pulse (5−8 ns). Thus, the transient observed upon excitation at 450 nm cannot be assigned to a monobrominated intermediate, as this would be inconsistent with the fast dynamics upon excitation at 355 nm. Additionally, assignment of the transient to the singlet excited state can be discarded because of the lack of fluorescence emission. Thus, the ∼50 ns transient is assigned

DOI: 10.1021/jacs.5b11649
J. Am. Chem. Soc. 2016, 138, 2678−2689

Scheme 3. (a) Chemical Mechanism of Bromine Photoelimination from PT-R-Br_2; (b) Proposed Photochemical and Photophysical Mechanisms for PT-R-Br_2 upon Excitation at 450 nm; (c) Proposed Photophysics of PT-R upon Excitation at 355 nm

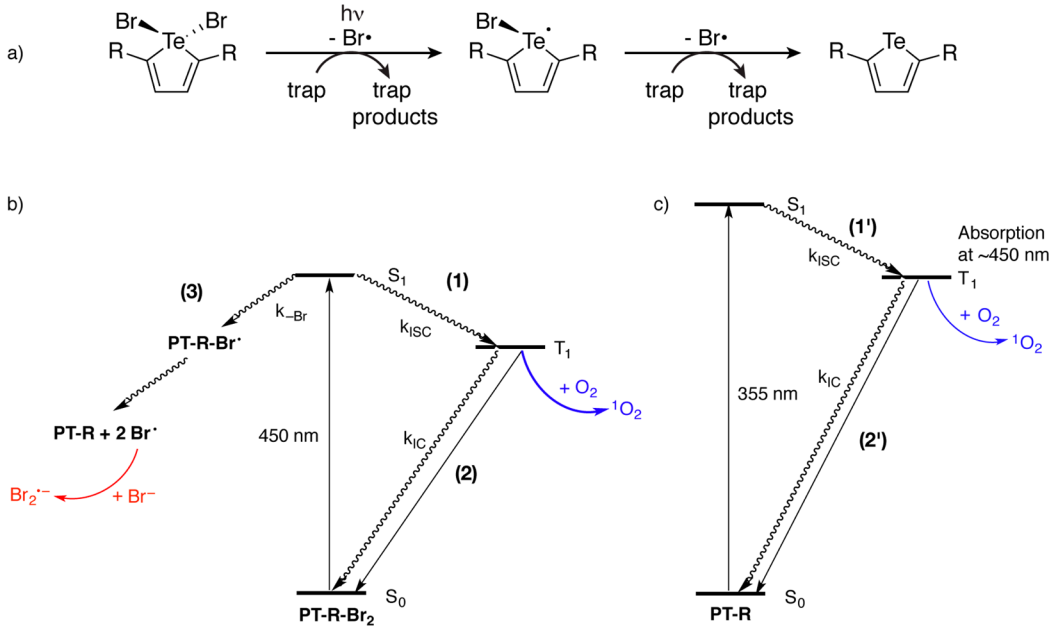

to the **PT-R-Br_2** triplet state, the formation of which is competitive with the photoreaction and is supported by the observation of phosphorescence and $^1O_2$ generation.

3. CONCLUSIONS

A series of substituted diphenyltellurophene compounds have been synthesized, and the reactivity of these compounds has been evaluated in terms of oxidative addition and photoelimination of bromine. Density functional theory calculations support a dissociative mechanism for oxidative addition of Br_2 that involves the formation of an η^1 association complex, a monobrominated intermediate, and finally the dibrominated product. Photoelimination of bromine is induced through excitation into the low-energy absorption band using blue or red light-emitting diodes. The photochemical quantum yield increases with increasing electron-withdrawing character of the substituents, with a value of up to 42% achieved for the perfluorophenyl-substituted tellurophene at an alkene trap concentration of 5 M. The photoelimination reaction occurs from the S_1 excited state via elimination of two bromine radicals, as confirmed by trapping experiments. However, the photoreaction is competitive with intersystem crossing to the triplet state, as evidenced by the formation of singlet oxygen during photolysis under aerobic conditions. The results of these studies establish a mechanism for the efficient photoelimination of bromine from conjugated tellurophenes.

■ ASSOCIATED CONTENT

Supporting Information

The Supporting Information is available free of charge on the ACS Publications website at DOI: 10.1021/jacs.5b11649.

Experimental details, titration and photolysis data for all compounds, additional figures for the DFT mechanistic study, GC−MS data, additional figures for the LFP experiments, NMR spectra for all compounds, further discussion of trap products, and DFT-optimized geometry coordinates and absolute energies (PDF)
Crystallographic data for **PT-C_6F_5-Br_2** (CIF)
Crystallographic data for **PT-CF_3-Br_2** (CIF)
Crystallographic data for **PT-O*t*Bu-Br** (CIF)
Crystallographic data for **PT-*t*Bu-Br_2** (CIF)

■ AUTHOR INFORMATION

Corresponding Authors

*scaiano@photo.chem.uottawa.ca
*dseferos@chem.utoronto.ca

Notes

The authors declare no competing financial interest.

■ ACKNOWLEDGMENTS

D.S.S. is grateful to NSERC, DuPont for a Young Professor Grant, and the Alfred P. Sloan Foundation for a research fellowship in chemistry. E.I.C. is grateful to NSERC for a CGS D. We acknowledge the Canada Foundation for Innovation (Project 19119) and the Ontario Research Fund for funding of the Centre for Spectroscopic Investigation of Complex Organic Molecules and Polymers. We thank Mark Taylor for the use of his GC−MS instrument. A.E.L. and J.C.S. thank the Natural Sciences and Engineering Research Council of Canada, the Canada Research Chairs Program, and the Canada Foundation for Innovation for generous support.

■ REFERENCES

(1) Hoffmann, N. *Chem. Rev.* **2008**, *108*, 1052−1103.
(2) Heyduk, A. F.; Nocera, D. G. *Science* **2001**, *293*, 1639−1641.
(3) Nocera, D. G. *Inorg. Chem.* **2009**, *48*, 10001−10017.
(4) Elgrishi, N.; Teets, T. S.; Chambers, M. B.; Nocera, D. G. *Chem. Commun.* **2012**, *48*, 9474−9476.
(5) Powers, D. C.; Hwang, S. J.; Zheng, S.-L.; Nocera, D. G. *Inorg. Chem.* **2014**, *53*, 9122−9128.
(6) Esswein, A. J.; Veige, A. S.; Nocera, D. G. *J. Am. Chem. Soc.* **2005**, *127*, 16641−16651.

DOI: 10.1021/jacs.5b11649
J. Am. Chem. Soc. 2016, 138, 2678−2689

(7) Cook, T. R.; Esswein, A. J.; Nocera, D. G. *J. Am. Chem. Soc.* **2007**, *129*, 10094−10095.
(8) Teets, T. S.; Lutterman, D. A.; Nocera, D. G. *Inorg. Chem.* **2010**, *49*, 3035−3043.
(9) Teets, T. S.; Nocera, D. G. *J. Am. Chem. Soc.* **2009**, *131*, 7411−7420.
(10) Cook, T. R.; McCarthy, B. D.; Lutterman, D. A.; Nocera, D. G. *Inorg. Chem.* **2012**, *51*, 5152−5163.
(11) Powers, D. C.; Chambers, M. B.; Teets, T. S.; Elgrishi, N.; Anderson, B. L.; Nocera, D. G. *Chem. Sci.* **2013**, *4*, 2880−2885.
(12) Cook, T. R.; Surendranath, Y.; Nocera, D. G. *J. Am. Chem. Soc.* **2009**, *131*, 28−29.
(13) Lin, T.-P.; Gabbaï, F. P. *J. Am. Chem. Soc.* **2012**, *134*, 12230−12238.
(14) Yang, H.; Gabbaï, F. P. *J. Am. Chem. Soc.* **2014**, *136*, 10866−10869.
(15) Hwang, S. J.; Powers, D. C.; Maher, A. G.; Anderson, B. L.; Hadt, R. G.; Zheng, S.-L.; Chen, Y.-S.; Nocera, D. G. *J. Am. Chem. Soc.* **2015**, *137*, 6472−6475.
(16) Karikachery, A. R.; Lee, H. B.; Masjedi, M.; Ross, A.; Moody, M. A.; Cai, X.; Chui, M.; Hoff, C. D.; Sharp, P. R. *Inorg. Chem.* **2013**, *52*, 4113−4119.
(17) Perera, T. A.; Masjedi, M.; Sharp, P. R. *Inorg. Chem.* **2014**, *53*, 7608−7621.
(18) Wickramasinghe, L. A.; Sharp, P. R. *Inorg. Chem.* **2014**, *53*, 1430−1442.
(19) Wickramasinghe, L. A.; Sharp, P. R. *J. Am. Chem. Soc.* **2014**, *136*, 13979−13982.
(20) Jahnke, A. A.; Howe, G. W.; Seferos, D. S. *Angew. Chem., Int. Ed.* **2010**, *49*, 10140−10144.
(21) Jahnke, A. A.; Seferos, D. S. *Macromol. Rapid Commun.* **2011**, *32*, 943−951.
(22) Jahnke, A. A.; Djukic, B.; McCormick, T. M.; Buchaca Domingo, E.; Hellmann, C.; Lee, Y.; Seferos, D. S. *J. Am. Chem. Soc.* **2013**, *135*, 951−954.
(23) Lee, W.-H.; Lee, S. K.; Shin, W. S.; Moon, S.-J.; Kang, I.-N. *J. Polym. Sci., Part A: Polym. Chem.* **2013**, *51*, 2753−2758.
(24) Jung, E. H.; Bae, S.; Yoo, T. W.; Jo, W. H. *Polym. Chem.* **2014**, *5*, 6545−6550.
(25) Park, Y. S.; Kale, T. S.; Nam, C.-Y.; Choi, D.; Grubbs, R. B. *Chem. Commun.* **2014**, *50*, 7964−7967.
(26) Park, Y. S.; Wu, Q.; Nam, C.-Y.; Grubbs, R. B. *Angew. Chem., Int. Ed.* **2014**, *53*, 10691−10695.
(27) Takimiya, K.; Kunugi, Y.; Konda, Y.; Niihara, N.; Otsubo, T. *J. Am. Chem. Soc.* **2004**, *126*, 5084−5085.
(28) Kaur, M.; Yang, D. S.; Shin, J.; Lee, T. W.; Choi, K.; Cho, M. J.; Choi, D. H. *Chem. Commun.* **2013**, *49*, 5495−5497.
(29) Kaur, M.; Lee, D. H.; Yang, D. S.; Um, H. A.; Cho, M. J.; Kang, J. S.; Choi, D. H. *Chem. Commun.* **2014**, *50*, 14394−14396.
(30) Carrera, E. I.; Seferos, D. S. *Macromolecules* **2015**, *48*, 297−308.
(31) Rivard, E. *Chem. Lett.* **2015**, *44*, 730−736.
(32) Lapkowski, M.; Motyka, R.; Suwiński, J.; Data, P. *Macromol. Chem. Phys.* **2012**, *213*, 29−35.
(33) He, G.; Torres Delgado, W.; Schatz, D. J.; Merten, C.; Mohammadpour, A.; Mayr, L.; Ferguson, M. J.; McDonald, R.; Brown, A.; Shankar, K.; Rivard, E. *Angew. Chem., Int. Ed.* **2014**, *53*, 4587−4591.
(34) He, G.; Wiltshire, B. D.; Choi, P.; Savin, A.; Sun, S.; Mohammadpour, A.; Ferguson, M. J.; McDonald, R.; Farsinezhad, S.; Brown, A.; Shankar, K.; Rivard, E. *Chem. Commun.* **2015**, *51*, 5444−5447.
(35) Kryman, M. W.; Schamerhorn, G. A.; Yung, K.; Sathyamoorthy, B.; Sukumaran, D. K.; Ohulchanskyy, T. Y.; Benedict, J. B.; Detty, M. R. *Organometallics* **2013**, *32*, 4321−4333.
(36) Koide, Y.; Kawaguchi, M.; Urano, Y.; Hanaoka, K.; Komatsu, T.; Abo, M.; Terai, T.; Nagano, T. *Chem. Commun.* **2012**, *48*, 3091−3093.
(37) Kaur, M.; Yang, D. S.; Choi, K.; Cho, M. J.; Choi, D. H. *Dyes Pigm.* **2014**, *100*, 118−126.
(38) McCormick, T. M.; Carrera, E. I.; Schon, T. B.; Seferos, D. S. *Chem. Commun.* **2013**, *49*, 11182−11184.
(39) Annaka, T.; Nakata, N.; Ishii, A. *Organometallics* **2015**, *34*, 1272−1278.
(40) Mahrok, A. K.; Carrera, E. I.; Tilley, A. J.; Ye, S.; Seferos, D. S. *Chem. Commun.* **2015**, *51*, 5475−5478.
(41) Tsao, F. A.; Lough, A. J.; Stephan, D. W. *Chem. Commun.* **2015**, *51*, 4287−4289.
(42) Tsao, F. A.; Stephan, D. W. *Dalton Trans.* **2015**, *44*, 71−74.
(43) Tsao, F. A.; Cao, L.; Grimme, S.; Stephan, D. W. *J. Am. Chem. Soc.* **2015**, *137*, 13264−13267.
(44) Misra, S.; Chauhan, A. K. S.; Srivastava, R. C.; Butcher, R. J.; Duthie, A. *J. Organomet. Chem.* **2015**, *791*, 119−123.
(45) Ali, A. M. M.; Ramazanova, P. A.; Abakarov, G. M.; Tarakanova, A. V.; Anisimov, A. V. *Russ. J. Gen. Chem.* **2015**, *85*, 770−772.
(46) Detty, M. R.; Luss, H. R. *Organometallics* **1986**, *5*, 2250−2256.
(47) Detty, M. R.; Friedman, A. E. *Organometallics* **1994**, *13*, 533−540.
(48) Detty, M. R.; Friedman, A. E.; McMillan, M. *Organometallics* **1994**, *13*, 3338−3345.
(49) McCormick, T. M.; Jahnke, A. A.; Lough, A. J.; Seferos, D. S. *J. Am. Chem. Soc.* **2012**, *134*, 3542−3548.
(50) Carrera, E. I.; McCormick, T. M.; Kapp, M. J.; Lough, A. J.; Seferos, D. S. *Inorg. Chem.* **2013**, *52*, 13779−13790.
(51) Carrera, E. I.; Seferos, D. S. *Dalton Trans.* **2015**, *44*, 2092−2096.
(52) Detty, M. R. *Organometallics* **1991**, *10*, 702−712.
(53) Aprile, A.; Iversen, K. J.; Wilson, D. J. D.; Dutton, J. L. *Inorg. Chem.* **2015**, *54*, 4934−4939.
(54) Vilhelmsen, M. H.; Jensen, J.; Tortzen, C. G.; Nielsen, M. B. *Eur. J. Org. Chem.* **2013**, *2013*, 701−711.
(55) Mack, W. *Angew. Chem., Int. Ed. Engl.* **1966**, *5*, 896−896.
(56) Terao, Y.; Wakui, H.; Satoh, T.; Miura, M.; Nomura, M. *J. Am. Chem. Soc.* **2001**, *123*, 10407−10408.
(57) Terao, Y.; Wakui, H.; Nomoto, M.; Satoh, T.; Miura, M.; Nomura, M. *J. Org. Chem.* **2003**, *68*, 5236−5243.
(58) Peng, C.; Schlegel, H. B. *Isr. J. Chem.* **1993**, *33*, 449−454.
(59) Peng, C.; Ayala, P. Y.; Schlegel, H. B.; Frisch, M. J. *J. Comput. Chem.* **1996**, *17*, 49−56.
(60) Fukui, K. *Acc. Chem. Res.* **1981**, *14*, 363−368.
(61) Parker, C. A. *Proc. R. Soc. London, Ser. A* **1953**, *220*, 104−116.
(62) Hatchard, C. G.; Parker, C. A. *Proc. R. Soc. London, Ser. A* **1956**, *235*, 518−536.
(63) Kuhn, H. J.; Braslavsky, S. E.; Schmidt, R. *Pure Appl. Chem.* **2004**, *76*, 2105−2146.
(64) Tzerpos, N. I.; Zarkadis, A. K.; Kreher, R. P.; Repas, L.; Lehnig, M. *J. Chem. Soc., Perkin Trans. 2* **1995**, 755−761.
(65) Clennan, E. L.; Chen, X. *J. Am. Chem. Soc.* **1989**, *111*, 5787−5792.
(66) Anderson, J. E.; Doecke, C. W.; Pearson, H. *J. Chem. Soc., Perkin Trans. 2* **1976**, *1976*, 336−341.
(67) Wilkinson, F.; Helman, W. P.; Ross, A. B. *J. Phys. Chem. Ref. Data* **1993**, *22*, 113−262.
(68) Scaiano, J. C.; Barra, M.; Krzywinski, M.; Sinta, R.; Calabrese, G. *J. Am. Chem. Soc.* **1993**, *115*, 8340−8344.

DOI: 10.1021/jacs.5b11649
J. Am. Chem. Soc. 2016, 138, 2678−2689